ELSEVIER

Thin Solid Films 306 (1997) 86–91

thin solid films

Characterization of yttria-stabilized zirconia thin films grown by planar magnetron sputtering

Wen-Chou Tsai, Tseung-Yuen Tseng *

Department of Electronics Engineering and Institute of Electronics, National Chiao-Tung University, Hsinchu, Taiwan

Received 20 January 1997; accepted 30 April 1997

Abstract

Yttria-stabilized zirconia (YSZ) thin films were grown on Si by rf magnetron sputtering. Sputtering gun was positioned at various angles to the substrate normal to change the amount of plasma bombardment on the as-deposited films. YSZ films grown by off-axis sputtering (90°) are readily (200)-preferred orientated but the preferred orientation of the film is deteriorated when the growth angle is decreased and, consequently, plasma bombardment is increased due to the decreasing growth angles. The off-axis grown YSZ films exhibit atomically smooth interfaces, which are not observed for those films grown by on-axis sputtering. The variation of oxide charge with the growth angle is studied with the Al/YSZ/Si structure. The plasma bombardment plays an important role on the crystallinity and, therefore, the defect type of the films and is also considered to be responsible for the Si outdiffusion occurring in an on-axis grown film. © 1997 Elsevier Science S.A.

Keywords: Yttria-stabilized zirconia; Magnetron sputtering; Plasma bombardment; Thin films

1. Introduction

Zirconium oxide stabilized with yttria (YSZ) has long been investigated as a material for refractory use or oxygen sensor application. Recently, YSZ films appear to be the most popular choice as buffer layers on Si substrates for growing high-temperature superconductor (HTSC) films [1–3]. Applications of thin zirconia layers to metal–oxide–silicon (MOS) capacitors for advanced dynamic random access memory (DRAM) have also been investigated [4] and the results were feasible. Thus, understanding the properties of such oxide insulator–semiconductor capacitors is the important subject to the development of dielectric oxide application on silicon and HTSC.

Epitaxial YSZ films have been grown on Si by using pulsed laser deposition, ion-beam deposition and e-beam evaporation. From the aspect of mechanical simplicity and performance, sputtering serves to be a more compatible method for growing oxide films than the above techniques. Besides, sputtering is well used as a successful technique for growing large-area $YBa_2Cu_3O_7$ superconducting films. In this study, we explore YSZ thin films grown on Si by using magnetron sputtering with sputter gun positioned at various angles to the substrate normal. The effect of those angles on the crystallinity and electrical properties of the films is investigated.

2. Experimental

The YSZ films on n-type (100)Si wafers were grown by planar rf magnetron sputtering. The target used is a $(ZrO_2)_{0.9}(Y_2O_3)_{0.1}$ disk of about 5 cm in diameter sintered at 1400°C. The doping concentration of the Si substrate is 8×10^{15} cm^{-3} on the basis of the results of capacitance–voltage (C–V) measurement on MOS capacitors. The silicon substrates were chemically etched with dilute HF to remove native oxide before introduced into the vacuum chamber. The substrate temperature was maintained at 750°C and the total pressure was 6.6 Pa, which was maintained by a mixture of oxygen and argon at a flow rate ratio of 4/1. The sputtering gun can be positioned semicircularly over the substrate surface. Its locations were defined with the angle θ (°) measured from the normal of the substrate surface as shown in Fig. 1. Available angles are 0°, 40°, 60°, and 90°. The 0° is equivalent to on-axis sputtering geometry and the 90° is the exact off-axis

* Corresponding author. Tel.: +886-3-5731879; fax: +886-3-5724361; e-mail: tseng@cc.nctu.edu.tw.

PII S0040-6090(97)00282-4

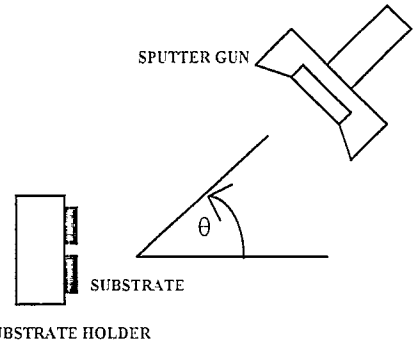

Fig. 1. Schematic diagram of the sputtering gun arrangement.

geometry. The deposition rates were 1.0, 0.5, 0.4, and 0.2 nm min^{-1} for $\theta = 0°$, 40°, 60°, and 90°, respectively. The deposition time duration was changed at various angles to obtain similar film thickness around 40 to 50 nm.

The crystallinity of the films was explored using X-ray diffraction (XRD) diagrams. The metal fractions of films and binding states of Y, Zr, and O were examined by electron spectroscopy for chemical analysis (ESCA, PHI1600, Physical Electronics, USA) with a resolution of 0.2 eV. The measured binding energies were calibrated using C 1s (assuming C 1s to be 284.6 eV) as the standard value. The structure and thickness of the films were determined by using transmission electron microscopy (TEM). For the electrical measurements, metal–insulator–semiconductor (MIS) capacitors of Al/YSZ/Si structure were employed and fabricated by depositing Al top electrodes on the YSZ films. Another Al layer was thermally evaporated on the backside of the Si wafer to form a back contact. The leakage current through the MIS capacitor was measured with HP4145B. The C–V curves of the MIS capacitors were obtained by using the Keithly CV82 system.

3. Results and discussion

All TEM results of the films show that the films are basically in polycrystalline cubic phase (JCPDS, No. 301468). Fig. 2 depicts the XRD diagrams of the films deposited at various angles to the substrate normal. The off-axis deposited films exhibit highly (200)-preferred orientation. The intensity of (200)YSZ diffraction peak decreases as the growth angle (θ)decreases. The on-axis grown film shows additional (111) diffraction peak, indicating that the crystalline orientation of the films gradually changes to multi-orientation as the angle decreases. What causes this change of film orientation? To obtain the possible answer, an assistant experiment was performed in which YSZ film were simultaneously deposited on two Si wafers, locating inside and outside the plasma region, respectively. The thickness of the films grown outside the plasma region is thinner (35 nm) than the thickness of the

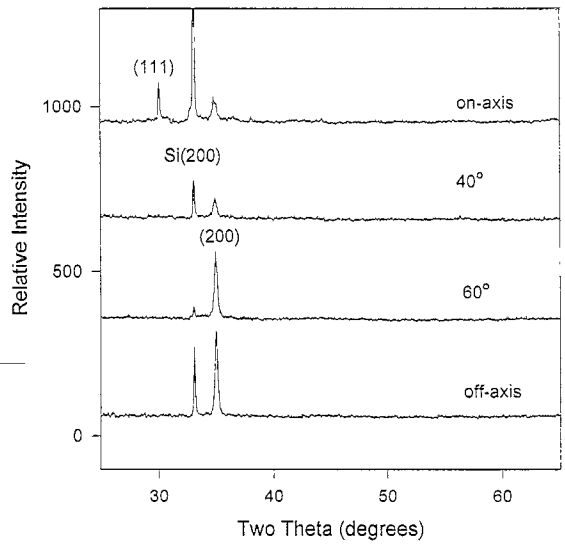

Fig. 2. XRD diagrams of the films grown at various angles.

inside plasma region (72 nm), however, XRD diagrams illustrate that the former exhibits much stronger diffraction intensity. The result of this additional experiment supports that low angle deposition may lead to enhanced plasma bombardment on the film surface and therefore, the preferred orientation of the film is deteriorated.

Fig. 3 shows XRD phi-scan diagrams of the films deposited at various angles. The diffraction was adjusted to explore the in-plane texturing of (200)-oriented YSZ grains. Zero degree phi in this figure was obtained by aligning the (311)Si diffraction. All the diagrams do not exhibit strong intensities, which reveals the polycrystallinity nature of the

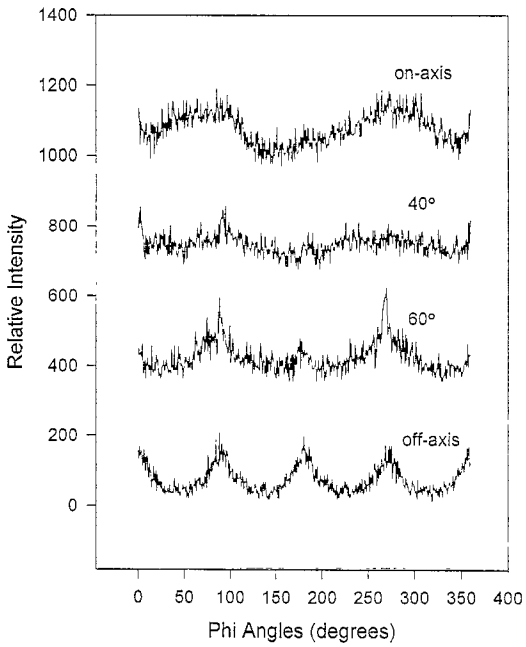

Fig. 3. XRD phi-scan diagrams of the films grown at various angles.

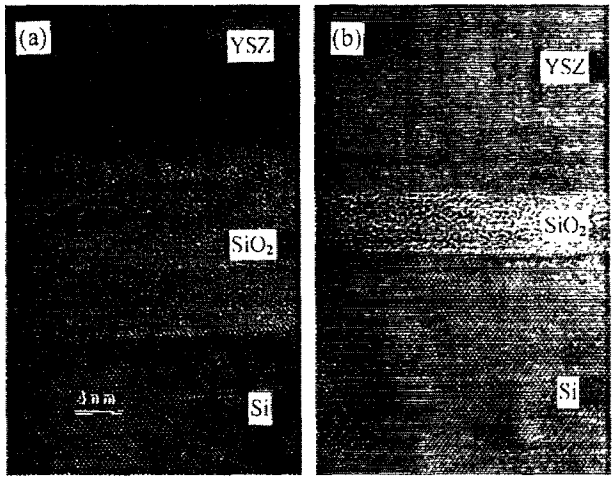

Fig. 4. Cross TEM images of the (a) on-axis and (b) off-axis grown films.

films. However, a four fold symmetry is observed on the diagrams of the off-axis grown films. This symmetry indicates that YSZ would generally grow on Si with a dominant in-plane orientation, which is (010)YSZ/(010)Si. This orientation relationship is the same as that for the YSZ films grown on Si by using other methods such as pulsed-laser deposition or ion-beam deposition [2,5]. This figure also shows that the tendency for four fold symmetry decreases as the angle decreases, which reflects the deteriorated crystallinity and twist alignment of the low angle grown films. Furthermore, the (111)-oriented grains in the on-axis grown films as illustrated in Fig. 2, do not depict in-plane texturing on Si as examined by XRD phi-scan. The reason to explain the randomly in-plane texturing is also attributed to the plasma bombardment which may heavily destroy the orientation relationship at the initial growth.

The cross sectional TEM images of Fig. 4 indicate that a SiO_2 layer forms between the YSZ film and Si. The formation of an intermediate amorphous SiO_2 layer has also been reported on epitaxial YSZ film grown on Si [2,6,7]. Since it was found that the oxide on Si surface must be removed to allow the epitaxial growth of YSZ films occurring, therefore, this SiO_2 layer must have formed after the growth of YSZ was established. On the other hand, this formation is expected in view of the high oxygen ion conductivity of the YSZ, indicating a high oxygen mobility. The thickness of SiO_2 layer increases with the decreasing angle, which are around 52 and 140 Å for the off-axis and on-axis grown films, respectively. The duration time for on-axis sputtering is the shortest but leading to the formation of the thickest SiO_2 layer. Obviously, the deposition time cannot explain the thickness variation of SiO_2 layer. Plasma bombardment may enhance the oxidation of Si. Possible causes responsible for the enhanced oxidation may be attributed to the higher concentration of active oxygen atoms/ions within plasma happened at on-axis growth. On the other hand, the increase of surface temperature of the substrates due to plasma bombardment may also be one of the contributing factors but the actual temperature rise on the substrate surface is hard to estimate. The YSZ/SiO_2 interface of the off-axis grown film shown in Fig. 4 is atomically smooth and clear whereas that of the on-axis grown film is slightly rough and unclear. The rougher interface as shown in Fig. 4a implies that the initial film growth, which plays an important role on determining the crystallinity and orientation of the whole films, is heavily disturbed by plasma bombardment and thus results in randomly oriented grains and rough interfaces. Besides, the slight unclear YSZ/SiO_2 interface implies that possible interdiffusion occurs between Si and YSZ due to plasma bombardment. This interdiffusion will be further discussed later.

Fig. 5 shows the variation of Y to Zr atomic ratios of the films with growth angles. The atomic ratios were obtained by using ESCA examination. The Y/Zr atomic ratio of the film increases with increasing angle. The Y/Zr ratio of on-axis grown film is around 0.12 whereas that of off-axis grown film is 0.22 which is the same as that of the target. Apparently, the Y atom is more easily resputtered than Zr under plasma bombardment. The Y resputtering enhanced by plasma bombardment has been observed in Y_2O_3 film deposition as well [8]. However, the change of Y/Zr ratio does not vary the YSZ cubic structure. Fig. 5 also shows the lattice constant of the films. The higher Y/Zr ratio provided at larger growth angles generally results in larger lattice constant. The trend is similar to that for bulk YSZ [9].

The variation of the atomic binding state due to plasma bombardment was explored by using ESCA measurement and is shown in Fig. 6. The binding energy of Zr 3d is same for all the films and is exactly the value of ZrO_2. But the binding energy of Y 3d for the films is 0.3–0.5 eV larger than the reported value of Y_2O_3 (156.4 eV, [10]) and slightly increases with the increasing growth angles. This slight increase of binding energy is suggested due to the

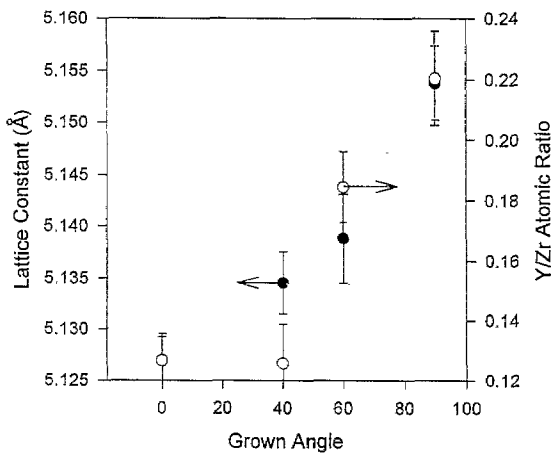

Fig. 5. Lattice constants (close symbols) and Y to Zr atomic ratios (open symbols) of the films grown at various angles.

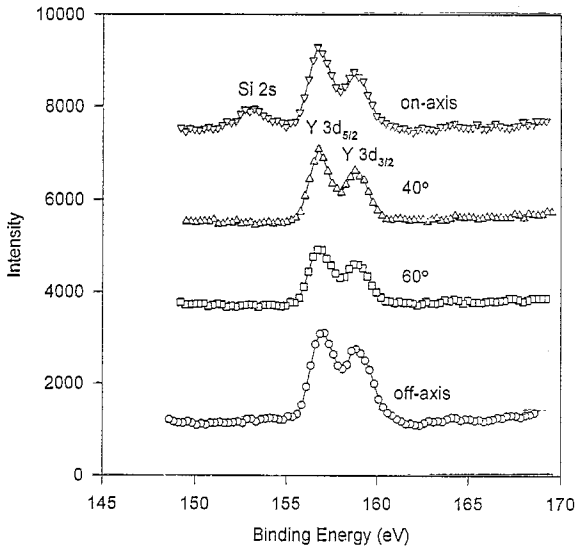

Fig. 6. Binding energies of Y 3d for the films grown at various angles.

increased substitution Y^{3+} for Zr^{4+} (Fig. 5). The introduction of Y atoms in zirconia is associated with the introduction of oxygen vacancies, which are created to preserve the electrical neutrality. In fact, the formation of oxygen vacancies decreases the average coordination number of yttrium ions, which should result in an increased bond strength and consequently an increased binding energy. However, this evidence implies that the atoms keep similar binding state in spite of the plasma bombardment effect. In addition, there is a Si 2s peak at 153.2 eV for the on-axis grown film [7,10], and no such peak is observed for the other films. Obviously, the Si outdiffused from the substrate during processing may occur. This binding energy of Si 2s is close to that of bulk Si. The unclear interface of YSZ/SiO_2 as shown in Fig. 4a also implies that Si may out-diffuse from the substrate with the aid of plasma bombardment at the beginning of the thin film growth. In our previous study, we also found that Si has existed in on-axis sputtered $(Zr_{0.7}Sn_{0.3})TiO_4$ films on Si substrate [11].

The leakage current through the MIS capacitor was measured at positive biased voltage to eliminate the influence of space-charge depletion region near the Si surface. Fig. 7 shows that the leakage current through MIS capacitors increases with increasing growth angles. Most of the MIS capacitors exhibit leakage current of the order of 10^{-7} A cm^{-2} at 1 MV cm^{-1}. However, the MIS capacitor with off-axis grown film exhibits leakage current three orders higher than the others. This phenomenon can be partly explained as due to the thinner SiO_2 layer formed in off-axis grown YSZ/Si interface as stated previously. It has been reported that amorphous SiO_2 was better insulating than stabilized zirconium oxide with high dielectric constants [9,12]. Thus, the existence of SiO_2 layer results in the lower leakage current through the MIS capacitors except for off-axis grown films. The thicker SiO_2 results in smaller leakage current. Electrons are expected to tunnel through the 5 nm thick SiO_2 layer existed in off-axis grown YSZ/Si interface under moderate biased voltage. Thus the leakage current curve for the off-axis grown film could reveal the real electrical conduction property of pure YSZ films, less disturbed by that of the SiO_2 layer. The leaky property of YSZ layer shown in Fig. 7 is possibly due to the ionic conduction of YSZ. In addition, structural variation of the films can also contribute to the leakage current change. It was generally observed that amorphous films exhibit lower leakage current than crystalline or preferred oriented films [13]. From this viewpoint, the leakage current change through the films as shown on Fig. 7 is in accordance with the crystalline change as shown on Fig. 2. The current–voltage curves of the films show ohmic conduction characteristics at low applied voltages (< 10 V) and follow a power-law relationship at higher voltages. This phenomenon at high voltage was well observed in many oxide films and could be ascribed to space-charge-limited current conduction [14].

Fig. 8 illustrates the C–V curves measured on the films grown at various angles. The MIS capacitors with various angle grown films depict typical MIS C–V curves under measurements, that is, with accumulation, depletion, and inversion regions, except the off-axis grown film, which is expected to result from the high electrical conductivity of the off-axis grown film as shown on Fig. 7. Table 1 lists electrical properties of the films calculated from C–V measurements. The dielectric constants of YSZ layers are obtained by applying the oxide capacitance (in accumulation region) to a parallel-plate capacitor model and deleting the effect of SiO_2 layer. The film grown at 40° exhibits the highest dielectric constant, whereas the on-axis grown film the lowest dielectric constant.

Another feature illustrated in Fig. 8 is the shift of the

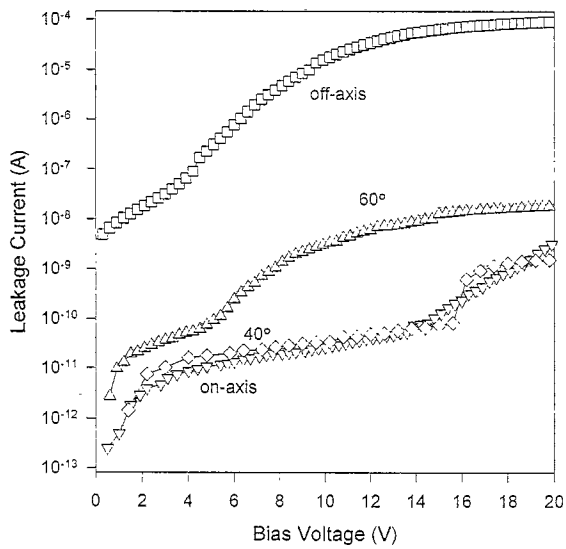

Fig. 7. Leakage current versus gate bias voltage for the films grown at various angles.

$C-V$ curves. The $C-V$ curves of the films negatively shift as the growth angle decreases. This shift corresponds to the variation of flatband voltage V_{FB}, which is related to oxide charge density caused by the defects existing in the films [12]. Table 1 depicts that the films grown at lower angles exhibit larger negative V_{FB} values. The on-axis grown film exhibits the largest negative V_{FB} and, thus, the highest density of positive oxide charge, which is due to the worst crystallinity as illustrated in Fig. 2. The worse crystallinity of the film can result in more defect, thus, more trapped charges. On the other hand, the oxide charge in SiO_2 layer may be significant because it is amorphous. If SiO_2 exhibits positive oxide charge, the variation of SiO_2 thickness with growth angles for the film could partly account for V_{FB} shift. Further investigations are necessary to elucidate the origin of the V_{FB} shift. It is indicated that V_{FB} is negative for the films grown at 40° and on-axis but it becomes positive for films grown at 60°, which means that 60° grown film exhibits net negative oxide charge. Therefore, the dominant defect type (i.e., trapped charge) in the oxide may change with the growth angles. Several explanations have been proposed to account for the positive shift of V_{FB} such as negatively charged ionic species present in the insulator, which were incorporated from the plasma during deposition, changes in the barrier height between the metal–insulator and/or insulator–insulator interfaces, and existence of interface states filled with electrons [15]. Considering that the YSZ film is an oxygen ion-conductor, another possible origin of the negative charge would be oxygen ions in the YSZ film.

Table 1 also lists interface–state–charge density (Nss) of the films, which characterizes the interface state charge on Si for a MIS capacitor. It is calculated from the slope of the $C-V$ curve at V_{FB} by using the formula reported by Lehovec [16]. Nss is lower for the film grown at lower angles as Table 1 depicted. This trend is different from that of V_{FB}. Therefore, the interface state charge would not be the dominant charge contributing to V_{FB} shift. The SiO_2/Si interface is considered to contribute to Nss more than the YSZ/SiO_2 interface does because the former is closer to the substrate. It has been conjectured that the interfacial SiO_2 layer releases the -6% lattice mismatch between YSZ and Si, which otherwise would presumably result in an increased number of interface traps [17]. In this study, Nss is of the order of 10^{11} eV^{-1} cm^{-2}, which is comparable with those of epitaxial YSZ/SiO_2 composite films on Si by other reports [17,18]. This comparison confirms that Nss is mainly contributed by the SiO_2/Si interface, not the YSZ/SiO_2 interface. The on-axis grown film exhibits the thickest SiO_2 and the lowest Nss. This result is in accordance with that obtained for CeO_2 films in which a thicker SiO_2 layer corresponded to lower Nss [19].

Table 1
The dielectric constant (ϵ), flatband voltage (V_{FB}), and interface state charge density (Nss) calculated from the $C-V$ curves of MIS capacitors with the films grown at various angles

Grown angle	ϵ	V_{FB} (V)	Nss (eV^{-1} cm^{-2})
60°	12.7	0.34	8.3×10^{11}
40°	13.2	−0.60	5.9×10^{11}
0°	10.0	−1.52	3.3×10^{11}

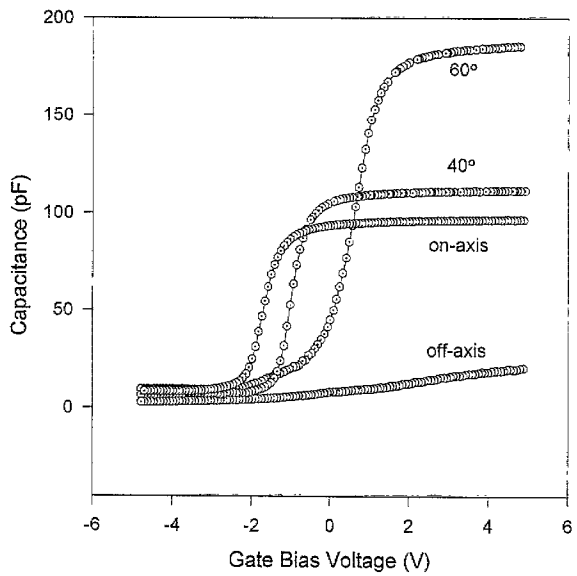

Fig. 8. $C-V$ curves of the films grown at various angles.

4. Summary

Effects of plasma bombardment on as-deposited YSZ films by sputtering were explored with the sputter gun located at various angles to substrate normal. The crystallinity and electrical properties of the films change with the growth angles. The (200)-preferred orientation films can be grown by off-axis sputtering. As the growth angle decreased, the films exhibited (111)-oriented grains, which is attributed to increasing plasma bombardment. The off-axis grown film, not deposited under plasma bombardment, exhibits atomically smooth interfaces with SiO_2 layer. The on-axis grown film exhibits positive oxide charge in total but the film grown at 60° reveals characteristics of negative oxide charge. Characteristics of MOS diodes with YSZ films as gate oxide show that the SiO_2 layer plays an important role in transport properties of the diode. These results show that plasma bombardment induced by lower growth angle significantly affects the growth and properties of the YSZ thin film on Si.

Acknowledgements

We acknowledge the support from National Science Council of ROC under contract No. NSC 85-2112-M009-037 PH.

References

[1] H. Nasu, H. Myoren, Y. Ibrar, S. Makida, Y. Nishiyama, T. Kato, T. Imura, Y. Osaka, Jpn. J. Appl. Phys. 27 (1988) L634.

[2] D.K. Fork, D.B. Fenner, A. Barrera, J.M. Phillips, T.H. Geballe, G.A.N. Connell, J.B. Boyce, IEEE Trans. Appl. Supercond. 1 (1991) 67.

[3] W. Prusseit, S. Corsépius, M. Zwerger, P. Berberich, H. Kinder, O. Eibl, C. Jaekel, U. Breuer, H. Kurz, Physica C 201 (1992) 249.

[4] J. Shappir, A. Anis, I. Pinsky, IEEE Trans. Electron Devices ED-33 (1986) 442.

[5] T. Matthée, J. Wecker, H. Behner, G. Friedl, O. Eibl, K. Samwer, Appl. Phys. Lett. 61 (1992) 1240.

[6] A. Lubig, Ch. Buchal, D. Guffi, C.L. Jia, B. Stritzker, Thin Solid Films 217 (1992) 125.

[7] D.B. Fenner, A.M. Viano, D.K. Fork, G.A.N. Connell, J.B. Boyce, F.A. Ponce, J.C. Tramontana, J. Appl. Phys. 69 (1991) 2176.

[8] Y. Kageyama, Y. Taga, J. Vac. Sci. Technol. A9 (1991) 604.

[9] D.W. Strickler, W.G. Carlson, J. Am. Ceramic Soc. 47 (1964) 122.

[10] L.D. Schmidt, Handbook of X-ray Photoelectron Spectroscopy, Perkin-Elmer, MN, 1978.

[11] F.J. Wu, T.Y. Tseng, J. Am. Ceram. Soc. in press.

[12] S.M. Sze, Physics of Semiconductor Devices, 2nd Edn., Wiley, New York, 1981, pp. 395.

[13] J.G. Simmons, Electronic conduction through thin insulating film, In: L.I. Maissel, R. Glang (Eds.), Handbook of Thin Film Technology, McGraw-Hill, New York, 1970, p. 14-1.

[14] S.B. Krupanidhi, M. Sayer, Thin Solid Films 113 (1984) 173.

[15] Y. Miyahara, J. Appl. Phys. 71 (1992) 2309.

[16] K. Lehovec, Solid State Electronics 11 (1968) 135.

[17] E.M. Ajimine, F.E. Pagaduan, M.M. Rahman, C.Y. Yand, H. Inokasa, D.K. Fork, T.H. Geballe, Appl. Phys. Lett. 59 (1991) 2889.

[18] C. Pellet, C. Schwebel, P. Hesto, Thin Solid Films 175 (1989) 23.

[19] W.C. Tsai, T.Y. Tseng, J. Mater. Sci. Mater. Electronics, in press.